A relativistic spin-polarised multiple-scattering theory, with applications to the calculation of the electronic structure of condensed matter

1989 J. Phys.: Condens. Matter 1 2959

(http://iopscience.iop.org/0953-8984/1/18/002)

J. Phys.: Condens. Matter 1 (1989) 2959–2975. Printed in the UK

A relativistic spin-polarised multiple-scattering theory, with applications to the calculation of the electronic structure of condensed matter

P Strange†‡, H Ebert†§, J B Staunton¶ and B L Gyorffy†

† Physics Department, Bristol University, Tyndall Avenue, Bristol BS8 1TL, UK

¶ Physics Department, Warwick University, Coventry, West Midlands, UK

Received 10 August 1988, in final form 28 October 1988

Abstract. A fully relativistic spin-polarised multiple-scattering theory is described for solving the fundamental Kohn–Sham equations of the relativistic spin-density functional theory. Particular attention is paid to calculating the Green functions for the Dirac-like equations occurring in the theory. Practical ways of evaluating the appropriate formulae are discussed and illustrated by explicit calculations of energy bands, density of states, and spin contribution to the magnetic moment in ferromagnetic iron. The difference between this fully relativistic theory and previous treatments of relativistic effects in magnetic materials is emphasised. Several physical applications of the method are suggested.

1. Introduction

Compared with a non-relativistic description, relativistic quantum mechanics of electrons in condensed matter has a number of qualitatively new features. One of these is the coupling between the spin and orbital degrees of freedom. Evidently its consequences are particularly striking in spin-polarised systems of itinerant electrons such as occurs in metallic magnets. For instance, it is this coupling that gives rise to the magnetocrystalline anisotropy energy (Landau *et al* 1984, March *et al* 1984, Staunton *et al* 1988) and is responsible for the different response of a spin-polarised system of electrons to left-handed and right-handed circularly polarised x-rays (Schutz *et al* 1987). In a previous paper (Strange *et al* 1984) we took the first steps towards a first principles theory of electrons in condensed matter including both relativity and magnetism on an equal footing. In that paper we discussed relativistic spin-polarised single-site scattering theory only. Independently an equivalent theory was set up by Feder *et al* (1983) and Feder (1985).

In the present paper we briefly discuss relativistic density functional theory, the single-site Green function, and derive the multiple-scattering Green function for a crystalline array of scattering centres. A similar expression has been derived by Schadler *et al* (1987). Furthermore, the calculation of observables from the Green function is outlined and then the practical aspects of the corresponding calculation are discussed.

‡ Present Address: Neutron Division, Rutherford Appleton Laboratory, Chilton, Didcot, Oxfordshire OX11 0QX, UK

§ Present Address: Siemens AG, ZFE-TPH 11, Paul-Gossen Strasse 100, D-8520 Erlangen, Federal Republic of Germany

0953-8984/89/182959 + 17 $02.50

We only mention those problems that do not occur in more conventional band theories. Finally, the theory is illustrated with a calculation of the energy bands, density of states and spin contribution to the magnetic moment of ferromagnetic iron.

2. Relativistic density functional theory

It is now well established that the equilibrium properties of many-electron systems can be usefully described by density functional theory (Kohn and Vashista 1983). In this approach the complicated many-body problem is reduced to a set of effective single-particle Schrödinger-like equations for which the effective potential is a functional of the charge and magnetisation densities and therefore has to be solved self-consistently. In this theory the so-called many-body effects are described by the exchange and correlation contribution to the effective potential functional. In practical applications these are treated in some local approximation (see Hedin and Lundqvist 1972, for example). Recently this theory has been generalised in order to make it applicable to systems in which relativity plays a significant role (Rajagopal 1978, MacDonald and Vosko 1979, Ramana and Rajagopal 1979). In particular, MacDonald and Vosko developed the theory for a many-electron system in the presence of an external potential and a 'spin-only' magnetic field (neglecting diamagnetic effects). Evidently a complete account of the relativistic effects mentioned in the introduction must be based on this framework. In this approximation the appropriate Kohn–Sham–Dirac equations which must be solved self-consistently are

$$(-ihc\boldsymbol{\alpha}\cdot p + \boldsymbol{\beta}mc^2 + \mathbf{I}\cdot V^{\text{eff}}[n(\boldsymbol{r}), m(\boldsymbol{r})] + \boldsymbol{\beta}\boldsymbol{\sigma}\cdot B^{\text{eff}}[n(\boldsymbol{r}), m(\boldsymbol{r})] - E_i)\boldsymbol{\psi}_i(\boldsymbol{r}) = 0 \tag{2.1a}$$

$$n(\boldsymbol{r}) = \sum_i^{\text{occ}} \boldsymbol{\psi}_i^+(\boldsymbol{r})\boldsymbol{\psi}_i(\boldsymbol{r}) \tag{2.1b}$$

$$m(\boldsymbol{r}) = \sum_i^{\text{occ}} \boldsymbol{\psi}_i^+(\boldsymbol{r})\boldsymbol{\beta}\boldsymbol{\sigma}\boldsymbol{\psi}_i(\boldsymbol{r}) \tag{2.1c}$$

$$V^{\text{eff}}[n(\boldsymbol{r}), m(\boldsymbol{r})] = -\left(V^{\text{ext}}(\boldsymbol{r}) + \frac{\delta E^{\text{xc}}[n(\boldsymbol{r}), m(\boldsymbol{r})]}{\delta n(\boldsymbol{r})} + e^2\int \frac{n(\boldsymbol{r}')}{|\boldsymbol{r}-\boldsymbol{r}'|}\,\mathrm{d}\boldsymbol{r}'\right) \tag{2.1d}$$

$$B^{\text{eff}}[n(\boldsymbol{r}), m(\boldsymbol{r})] = (eh/2mc)\{B^{\text{ext}}(\boldsymbol{r}) + \delta E^{\text{xc}}[n(\boldsymbol{r}), m(\boldsymbol{r})]/\delta m(\boldsymbol{r})\}. \tag{2.1e}$$

In equations (2.1) $\boldsymbol{\psi}_i(\boldsymbol{r})$ is a four-component one-electron Dirac spinor, $V^{\text{eff}}[n(\boldsymbol{r}), m(\boldsymbol{r})]$ is an effective potential which is the sum of three terms: an external potential $V^{\text{ext}}(\boldsymbol{r})$ due to the atomic nuclei, the relativistic exchange–correlation potential, and the classical electrostatic potential. Approximations for the exchange–correlation potential are discussed by MacDonald and Vosko (1979). Furthermore $\boldsymbol{\alpha}$ and $\boldsymbol{\beta}$ are the standard Dirac matrices, $\boldsymbol{\sigma}$ are the 4×4 Pauli matrices, E^{xc} is the relativistic exchange–correlation energy. $B^{\text{eff}}[n(\boldsymbol{r}), m(\boldsymbol{r})]$ is an effective magnetic field consisting of an exchange–correlation term and a fictional external magnetic field which couples to the spin of the electron only. All other symbols have their usual meanings and we work throughout in atomic units.

The above approximate equations are derived with the analogy with the non-relativistic limit in mind. A more general fully relativistic discussion of V^{eff} and B^{eff} is given by MacDonald and Vosko (1979). In the case of a solid, both $V^{\text{eff}}(\boldsymbol{r})$ and $B^{\text{eff}}(\boldsymbol{r})$ are a

sum of contributions from each site in the infinite lattice. A way of solving these equations was proposed by Feder *et al* (1983). Their approach was based on the layered KKR method of Pendry (1974). We follow the alternative approach of Strange *et al* (1984) and sum up the multiple scattering series in the conventional way, (Korringa 1947). For the sake of clarity, before studying the case of an infinite array of scatterers we summarise the single scatterer results of Strange *et al* (1984).

3. Single-site scattering theory

The first step towards deploying the multiple-scattering method to solve Dirac-like equations for non-overlapping arrays of potential wells is to solve the problem of a single well embedded in a constant background potential which we shall take as our energy zero.

Even for non-spherical targets the spin and angular dependence of the wavefunctions are most conveniently described by expansions in terms of the spin angular functions:

$$\chi_{\kappa}^{m_j}(\boldsymbol{r}) = \sum_{\sigma} C_{\sigma m_j - \sigma}^{\kappa m_j} Y_l^{m_j - \sigma}(\hat{\boldsymbol{r}}) X_{1/2}^{\sigma} \tag{3.1}$$

where $Y_l^m(\hat{\boldsymbol{r}})$ are the usual spherical harmonics, $X_{1/2}^{\sigma}$ is the spin function for total spin-$\frac{1}{2}$ and magnetic quantum number σ, the $C_{\sigma m_j - \sigma}^{\kappa m_j}$ are Clebsch–Gordon coefficients, m_j and κ are the eigenvalues of the angular momentum operator $\hat{J}_z$ and $\hat{K} = (\boldsymbol{\sigma} \cdot \hat{\boldsymbol{L}} + 1)$, respectively.

In terms of such expansions, outside the range of the potential well the following scattering solution may be defined

$$\boldsymbol{Z}_{\kappa'}^{m_j'}(r, p) = \sum_{\kappa m_j} \boldsymbol{J}_{\kappa}^{m_j}(p, r) t_{\kappa\kappa'}^{m_j m_j' - 1} + \boldsymbol{H}_{\kappa'}^{m_j'}(p, r) \tag{3.2}$$

where the four-component free-particle solutions $\boldsymbol{J}_{\kappa}^{m_j}$ and $\boldsymbol{H}_{\kappa}^{m_j}$ are given in terms of the spherical Bessel j_1 and Hankel h_1 functions as

$$\boldsymbol{J}_{\kappa}^{m_j}(p, \boldsymbol{r}) = \left(\frac{p(E+1)}{\pi}\right)^{1/2} \begin{bmatrix} j_1(pr)\chi_{\kappa}^{m_j}(\hat{\boldsymbol{r}}) \\ \mathrm{i}pS_{\kappa}/(E+1)\; j_1(pr)\chi_{-\kappa}^{m_j}(\hat{\boldsymbol{r}}) \end{bmatrix} \tag{3.3}$$

$$\boldsymbol{H}_{\kappa}^{m_j}(p, \boldsymbol{r}) = \left(\frac{p(E+1)}{\pi}\right)^{1/2} \begin{bmatrix} h_1(pr)\chi_{\kappa}^{m_j}(\hat{\boldsymbol{r}}) \\ \mathrm{i}pS_{\kappa}/(E+1)\; h_1(pr)\chi_{-\kappa}^{m_j}(\hat{\boldsymbol{r}}) \end{bmatrix} \tag{3.4}$$

The magnitude of the momentum p is given approximately by $p = \sqrt{E}$ (Rose 1961). $S_{\kappa} = |\kappa|/\kappa$. The coefficient matrix of $\boldsymbol{J}_{\kappa}^{m_j}$ in equation (3.2) is the inverse of $t_{\kappa\kappa'}^{m_j m_j'}(E)$, which is an element of the single-site scattering t-matrix (Lloyd and Smith 1972). Note that equation (3.2) is the appropriate boundary condition for a scattering problem with a non-spherical scatterer. It should be interpreted as being the superposition of an outgoing scattered wave with amplitude normalised to $H_{\kappa}^{m_j}(\boldsymbol{p}, \boldsymbol{r})$ plus a sum of contributions to it from all possible incident waves $J_{\kappa}^{m_j}(\boldsymbol{p}, \boldsymbol{r})$.

Inside the region of the potential $Z_{\kappa}^{m_j}$ is defined as

$$Z_{\kappa}^{m_j}(E, \boldsymbol{r}) = \sum_{\kappa'} \begin{bmatrix} g_{\kappa'\kappa}^{m_j}(E, r)\chi_{\kappa}^{m_j}(\hat{\boldsymbol{r}}) \\ \mathrm{i}f_{\kappa'\kappa}^{m_j}(E, r)\chi_{-\kappa}^{m_j}(\hat{\boldsymbol{r}}) \end{bmatrix} \tag{3.5}$$

where $g^{m_j}_{\kappa'\kappa}$ and $f^{m_j}_{\kappa'\kappa}$ are the solutions of the four coupled partial differential equations

$$\frac{\delta}{\delta r}[rcf^{m_j}_{\kappa'\kappa}(E,r)] = \kappa' cf^{m_j}_{\kappa'\kappa}(E,r) - [E - V^{\text{eff}}(r)]rg^{m_j}_{\kappa'\kappa}(E,r) + B^{\text{eff}}(r)\sum_{\kappa''} G(\kappa'',\kappa',m_j)g^{m_j}_{\kappa''\kappa}(E,r) \tag{3.6a}$$

$$\frac{\delta}{\delta r}[rg^{m_j}_{\kappa'\kappa}(E,r)] = -\kappa' g^{m_j}_{\kappa'\kappa}(E,r) - \{[E - V^{\text{eff}}(r)]/c^2 + 1\}crf^{m_j}_{\kappa'\kappa}(E,r) - \frac{B^{\text{eff}}(r)}{c^2}\sum_{\kappa''} G(-\kappa''\kappa' m)crf^{m_j}_{\kappa''\kappa}(E,r) \tag{3.6b}$$

and two equations coming from interchanging κ' and κ. The total angular momentum J^2 has eigenvalues $j(j+1)$ and its projection along the z-axis J_z has eigenvalues m_j. $G(\kappa',\kappa,m)$ is given in terms of Clebsch–Gordon coefficients by $G(\kappa',\kappa,m) = C^{\kappa,m_j}_{\frac{1}{2}m_j-\frac{1}{2}}C^{\kappa,m_j}_{\frac{1}{2}m_j-\frac{1}{2}} - C^{\kappa'm_j}_{\frac{1}{2}m_j+\frac{1}{2}}C^{\kappa m_j}_{\frac{1}{2}m_j+\frac{1}{2}}$. It is useful to recall that

$$\kappa = 1 \qquad \text{for } j = (1 - \tfrac{1}{2})$$
$$\kappa = -1 - 1 \qquad \text{for } j = (1 + \tfrac{1}{2})$$

In general the radial equations in equation (3.6) are an infinite set of coupled equations. However, the l to $l+2$ coupling can be neglected (Feder *et al* 1983, Strange *et al* 1984) and hence we shall be interested only in the case where κ'' is restricted to the values l and $-1-l$.

As was shown by Strange *et al* (1984) the scattering t-matrix, $t^{m_j,m_j}_{\kappa,\kappa'}$, is defined by matching the two solutions for $Z^{m_j}_{\kappa}$ (equations 3.2 and 3.5) at the boundary of the potential. The off-diagonal matrix structure of the t-matrix comes from the fact that more than one incident wave scatters onto a single outgoing wave of unit amplitude. An alternative derivation of this off-diagonal t-matrix has been given by Ebert and Gyorffy (1987).

It is often useful to transform to a representation familiar from non-relativistic quantum mechanics, defined by the quantum numbers, l, m, and s. This is related to the κm_j representation by

$$Y^m_l(\hat{r})\chi^{\alpha}_{1/2} = \sum_{\substack{\kappa=l \\ =-l-1}} C^{\sigma m}_{\kappa m_j}\chi^{m_j}_{\kappa}(\hat{\boldsymbol{r}}) \tag{3.7}$$

in this representation

$$t_{l'm_j-\sigma,\sigma,l',m_j-\sigma'\sigma'}(E) = \sum_{\kappa\kappa'} C^{\sigma m_j-\sigma}_{\kappa m_j} t^{m_j}_{\kappa\kappa'}(E) C^{\sigma' m_j-\sigma'}_{\kappa' m_j}. \tag{3.8}$$

The new feature of these t-matrices is that they are off-diagonal in spin space. The various interesting properties of this t-matrix were exhaustively investigated by Strange *et al* (1984). However they did not explicitly study the corresponding Green function. Thus we shall do this here.

Let us begin by considering a single potential well centred on the nth lattice site. Instead of the differential equation

$$[\mathrm{i}hc\boldsymbol{\alpha}\cdot p + \boldsymbol{\beta}mc^2 + \mathbf{I}V^{\text{eff}}(r) + \boldsymbol{\beta}\boldsymbol{\sigma}\cdot B^{\text{eff}}(r)]\mathbf{G}^n(\boldsymbol{r},\boldsymbol{r}',E) = \mathbf{I}\delta(\boldsymbol{r}-\boldsymbol{r}') \tag{3.9}$$

we wish to start with the equivalent integral equation for the 4×4 bispinor Green function $\mathbf{G}^n(\boldsymbol{r}, \boldsymbol{r}', E)$; see Faulkner and Stocks (1980).

$$\mathbf{G}^n(\boldsymbol{r}, \boldsymbol{r}', E) = \mathbf{G}^0(\boldsymbol{r}, \boldsymbol{r}', E) + \iint \mathbf{G}^0(\boldsymbol{r}, \boldsymbol{r}'', E)t(\boldsymbol{r}'', \boldsymbol{r}''', E)\mathbf{G}^0(\boldsymbol{r}''', \boldsymbol{r}', E)\,\mathrm{d}\boldsymbol{r}'''\,\mathrm{d}\boldsymbol{r}'' \tag{3.10}$$

where $\mathbf{G}^n(\boldsymbol{r}, \boldsymbol{r}', E)$ is the Green function for an electron scattering from a single site at $\boldsymbol{R}_n$, and $\boldsymbol{r}$ and $\boldsymbol{r}'$ are in the vicinity of the scattering centre, with $|r'| \geqslant |r|$. $\mathbf{G}^0(\boldsymbol{r}, \boldsymbol{r}', E)$ is the relativistic 4×4 matrix free-electron Green function given by Rose (1961).

$$\mathbf{G}^0(\boldsymbol{r}, \boldsymbol{r}', E) = \begin{pmatrix} G^0_{11}(\boldsymbol{r}, \boldsymbol{r}', E) & G^0_{12}(\boldsymbol{r}, \boldsymbol{r}', E) \\ G^0_{21}(\boldsymbol{r}, \boldsymbol{r}', E) & G^0_{22}(\boldsymbol{r}, \boldsymbol{r}', E) \end{pmatrix} \tag{3.11}$$

with

$$G^0_{11}(\boldsymbol{r}, \boldsymbol{r}', E) = \mathrm{i}p(E+1)\sum_{\kappa m_j} h_1(pr)j_1(pr')\chi^{m_j}_{\kappa}(\hat{\boldsymbol{r}}) \otimes \chi^{m_j *}_{\kappa}(\hat{\boldsymbol{r}}') \tag{3.12a}$$

$$G^0_{12}(\boldsymbol{r}, \boldsymbol{r}', E) = -p^2 \sum_{\kappa m_j} S_\kappa h^-_{\bar{l}}(pr)j_{\bar{l}}(pr')\chi^{m_j}_{-\kappa}(\hat{\boldsymbol{r}}) \otimes \chi^{m_j *}_{\kappa}(\hat{\boldsymbol{r}}') \tag{3.12b}$$

$$G^0_{21}(\boldsymbol{r}, \boldsymbol{r}', E) = -G^0_{12}(\boldsymbol{r}, \boldsymbol{r}', E) \tag{3.12c}$$

$$G^0_{22}(\boldsymbol{r}, \boldsymbol{r}', E) = (E-1)/(E+1)G^0_{11}(\boldsymbol{r}, \boldsymbol{r}', E) \tag{3.12d}$$

$\bar{l} = l - S$, and $\otimes$ stands for outer product. Substituting this into (3.10) leads, eventually, to the following two equivalent expressions for the Green function:

$$\mathbf{G}^n(\boldsymbol{r}, \boldsymbol{r}', E) = -\mathrm{i}p \sum_{\kappa\kappa' m_j} Z^{m_j}_{\kappa}(p, \boldsymbol{r})t^{m_j}_{\kappa\kappa'}H^{+ m_j}_{1\kappa'}(p, r') \tag{3.13a}$$

$$\mathbf{G}^n(\boldsymbol{r}, \boldsymbol{r}', E) = \sum_{\kappa\kappa' m_j} Z^{m_j}_{\kappa}(p, \boldsymbol{r})t^{m_j}_{\kappa\kappa'}(E)Z^{+ m_j}_{\kappa'}(p, \boldsymbol{r}') - \sum_{\kappa m_j} Z^{m_j}_{\kappa}(p, \boldsymbol{r})J^{+ m_j}_{\kappa}(p, \boldsymbol{r}) \tag{3.13b}$$

where $\boldsymbol{r}$ and $\boldsymbol{r}'$ are in the vicinity of site n, and $t^{m_j}_{\kappa\kappa'}(E)$ is an element on the energy shell single-site scattering t-matrix.

$$t^{m_j}_{\kappa\kappa'}(E) = \iint J^{+ m_j}_{\kappa}(p, \boldsymbol{r}')t(\boldsymbol{r}', \boldsymbol{r}'', E)J^{m_j}_{\kappa'}(p, \boldsymbol{r}'')\,\mathrm{d}^3\boldsymbol{r}'\,\mathrm{d}^3\boldsymbol{r}''. \tag{3.14}$$

$H_{1\kappa}$ is a solution of the Dirac equation for $r < r_{mt}$ and matches onto $H^{m_j}_{\kappa}$ for $r \geqslant r_{mt}$. The derivation of these equations is straightforward and is analogous to the non-relativistic derivation of Faulkner and Stocks (1980), and therefore we do not reproduce it here.

4. Multiple scattering

The Green function for a system of scatterers can be written in the form (Faulkner and Stocks, 1980)

$$G(\boldsymbol{r}, \boldsymbol{r}', E) = G^n(\boldsymbol{r}, \boldsymbol{r}', E) + \iint G^n(\boldsymbol{r}, \boldsymbol{r}'', E)T_{nn}(\boldsymbol{r}'', \boldsymbol{r}''', E)G^n(\boldsymbol{r}''', \boldsymbol{r}', E)\,\mathrm{d}\boldsymbol{r}''\,\mathrm{d}\boldsymbol{r}'''. \tag{4.1}$$

Here T_{nn} is the element of the t-matrix for the system without the scatterer at the nth site. It can be written in terms of the scattering path operators for the system of all sites

with the nth removed, τ_n^{ij} (Gyorffy and Stott 1973) as

$$T_{nn} = \sum_{i \neq n} \sum_{j \neq n} \tau_n^{ij}. \tag{4.2}$$

The four-vector $H_\kappa^{m_j}(pr)$ diverges at the origin but is regular at all other points in space. Therefore it can be expanded in spherical Bessel functions when $\boldsymbol{r}$ is close to some other site m. Analogously to Faulkner and Stocks (1980), we have

$$H_\kappa^{m_j'}(p, r_n) = -ip \sum_{\kappa m_j} g_{\kappa' m_j' \kappa m_j}^{nm} J_\kappa^{m_j}(p, r_m). \tag{4.3}$$

This is a straightforward generalisation of the non-relativistic case, with the expansion coefficients $g_{\kappa' m_j' \kappa m_j}^{nm}$ given in terms of the usual ones by

$$g_{\kappa' m_j' \kappa m_j}^{nm} = \sum_{\sigma = \pm \frac{1}{2}} C_{\sigma m_j - \sigma}^{\kappa' m_j'} g_{l' m_j' - \sigma l m_j - \sigma}^{nm} C_{\sigma m_j - \sigma}^{\kappa m_j}. \tag{4.4}$$

The structure constants are given by the usual expression (see Stocks and Winter 1984, for example):

$$g_{l'm'lm}^{nm}(E) = -4\pi i^{l-l'}(\sqrt{E}) \sum_{l''m''} i^{l''} C_{LL''}^{L''} h_{l''}[\sqrt{E}|\boldsymbol{R}_n - \boldsymbol{R}_m|] Y_{l''}^{m''}(\boldsymbol{R}_n - \boldsymbol{R}_m) \tag{4.5a}$$

and

$$g_{l'm'lm}(\boldsymbol{q}, E) = (1/N) \sum_{nm} \exp[i\boldsymbol{q} \cdot (\boldsymbol{R}_n - \boldsymbol{R}_m)] g_{l'm'lm}^{nm}(E) \tag{4.5b}$$

where the $\boldsymbol{R}_i$ are lattice vectors. If we define

$$\tau_{\kappa' m_j' \kappa m_j}^{ij}(E) = \int\int \boldsymbol{J}_\kappa^{+m_j}(p, \boldsymbol{r}_i) T_{nn}(\boldsymbol{r}_i, \boldsymbol{r}_j, E) J_\kappa^{m_j}(p, \boldsymbol{r}_j) \, \mathrm{d}^3 \boldsymbol{r}_i \, \mathrm{d}^3 \boldsymbol{r}_j \tag{4.6}$$

we can show, analogously to Faulkner and Stocks,

$$\mathbf{G}(\boldsymbol{r}, \boldsymbol{r}', E) = \sum_{\kappa\kappa' m_j} Z_\kappa^{m_j}(p, \boldsymbol{r}) \tau_{\kappa' m_j' \kappa m_j}(E) Z_\kappa^{m_j' +}(p, \boldsymbol{r}') - \sum_{\kappa m_j} Z_\kappa^{m_j}(p, \boldsymbol{r}) J_\kappa^{m_j +}(p, \boldsymbol{r}'). \tag{4.7}$$

An element of the τ-matrix can be written as

$$\tau_{\kappa' m_j' \kappa m_j}(\boldsymbol{q}, E) = 1/N \sum_{ij} \exp[i\boldsymbol{q} \cdot (\boldsymbol{R}_i - \boldsymbol{R}_j)] \tau_{\kappa' m_j' \kappa m_j}^{ij}(E) \tag{4.8a}$$

with number of sites N and

$$\tau_{\kappa' m_j' \kappa m_j}^{ij}(E) = \int [t^{-1} \delta_{ij} - g^{ij}(\boldsymbol{q}, E)]_{\kappa' m_j' \kappa m_j}^{-1} \, \mathrm{d}^3 \boldsymbol{q}. \tag{4.8b}$$

If we vary the energy E there will be certain places where the determinant $\|[t^{-1} - g(\boldsymbol{q}, E)]\|$ passes through zero. At these energies $\tau_{\kappa' m_j' \kappa m_j}(E)$ and hence $G(\boldsymbol{r}, \boldsymbol{r}', E)$ diverge. At these energies there will be amplified scattered waves even with no incident electron. They form the eigenvalue spectrum or electronic band structure of the system.

Once we have found the Green function we can calculate observables such as the density of states

$$N(E) = -\frac{1}{\pi} \mathrm{Im} \int \mathrm{Tr}\, \mathbf{G}(\boldsymbol{r}, \boldsymbol{r}, E) \, \mathrm{d}^3 \boldsymbol{r} \tag{4.9}$$

and the magnetic moment

$$M(r) = -\frac{1}{\pi}\,\mathrm{Im}\int_0^{E_F} \mathrm{Tr}\,\boldsymbol{\beta\sigma}\mathbf{G}(r, r, E)\,\mathrm{d}E \tag{4.10}$$

where the trace is over spin space.

In this paper we do not perform charge self-consistent calculations but if we require the charge density it can be found from

$$n(r) = -\frac{1}{\pi}\,\mathrm{Im}\int_0^{E_F} \mathrm{Tr}\,\mathbf{G}(r, r, E)\,\mathrm{d}E. \tag{4.11}$$

5. Practical aspects of the theory

In this section we discuss the practical difficulties involved in the calculation of the KKR Green function. Good reviews of the technical aspects of electronic structure calculations are given by Loucks (1967) and by Stocks *et al* (1979). Topics covered by these authors will not be repeated here.

We divide this section of our paper into three parts. First we discuss the use of complex energy techniques. In particular we focus on how this affects the calculation of the KKR structure constants, and on what are the advantages of such methods for calculating observables from the KKR Green function. Second, we note that complex energy methods introduce a second solution of the Dirac equation which is irregular at the origin and we discuss how to solve the Dirac equation with a magnetic field term under such circumstances. Third, we analyse the τ-matrix of equation (4.8). We consider its symmetry, the size and degeneracy of τ and how to perform the Brillouin zone integrals to find $\tau^{ii'}_{\Lambda,\Lambda}$ in a relativistic spin-polarised framework. Finally, we briefly discuss the optimum method for finding the eigenvalue spectrum from τ.

5.1. Complex energies

For a regular array of scatterers the τ-matrix as given by equation (4.8) is a very highly structured function of the energy E. This is reflected in the rapidly varying features of the densities of states. For an example, see § 6 for the density of states of iron. Computational efficiency can be improved by working at complex energies (Zeller *et al* 1982).

There are many methods used for calculating the KKR structure constants of equation (4.5). The summations can be done in real space or reciprocal space, or optimally, using the Ewald technique (see Davis 1971, for example), a mixture of both. We have found that at the complex energies that we use, the Ewald method is always the most efficient method.

We are unaware of any tabulated values of KKR structure constants at complex energies so our routines were checked by insisting that structure constants calculated by the Ewald technique agreed at several randomly chosen energies and wavevectors with those calculated using equation (4.5) at complex energies. Further details of this part of the calculation may be found elsewhere (Strange *et al* 1987).

For complex energy $z = E + \mathrm{i}\Gamma$ the Green function $G(\boldsymbol{r}, \boldsymbol{r}', z)$ can be written in terms of its value on the real axis:

$$G(\boldsymbol{r}, \boldsymbol{r}' E + \mathrm{i}\Gamma) = \frac{1}{\pi}\int_{-\infty}^{+\infty} \mathrm{d}E'\,\frac{\Gamma}{(E - E') + \Gamma^2}\,\mathrm{Im}\,G(\boldsymbol{r}, \boldsymbol{r}', E'). \tag{5.1}$$

$G(\boldsymbol{r}, \boldsymbol{r}'z)$ is analytic on the whole complex plane except for the real axis where it has a series of poles. All structure on the real axis is broadened when we go out on the complex plane by a Lorentzian of half-width Γ. Zeller *et al* (1982) have shown the density of states of nickel as a function of increasing imaginary energy Γ. They show that the density of states is almost flat well before $\Gamma - 0.5$ Ryd. Thus we require far fewer energy points to obtain an accurate value of the energy integrals in (4.10) and (4.11) for example.

The actual choice of complex path used in the calculations has to be a compromise. If $\Gamma \rightarrow \infty$ then the integrand in (4.10) or (4.11) would be flat and trivial to integrate. However, it is also desirable to have as short a path as possible. Koenig *et al* (1973) choose a straight line $E_F \pm i\Gamma$ which is completed by an infinite half semi-circle which can be calculated analytically and is often a vanishingly small contribution. We have followed the procedure of Zeller *et al* (1982) and used a rectangular contour from below the bottom of the valence band to the Fermi energy E_F. We have found an imaginary part of the energy between 0.05 and 0.10 Ryd sufficient for all purposes.

If the density of states is calculated on the real axis, E_F can be found as the energy at which the integrated density of states is equal to the correct number of electrons. At complex energies it is not clear at which value of the real energy one should return to the real axis. In our case this is done by estimating E_F and returning to 1 mRyd above the real axis. Then the density of states at several points parallel to the real axis is found and the integrated density of states is interpolated back to the real axis using the Cauchy–Riemann formula. The integrated density of states is the quantity used for the interpolation as it is the smoothest varying quantity in the calculation.

One price that we have to pay for the vastly increased computational efficiency complex energy techniques bring is that the imaginary part of the second term in the Green function of equation (4.7) is no longer zero and must be included in the calculation.

One final point to note in this section is that we often compare the results of electronic structure calculations with experimental observations which are limited by instrumental or temperature broadening. In such cases it may be that the results at carefully chosen values of the complex energy are sufficient and it is not necessary to return to the real axis.

5.2. *Solution of the radial Dirac equation in a magnetic field at complex energies*

In implementing the calculations discussed in previous sections it is necessary to solve the Dirac equation with a magnetic field term at complex energies. At complex energies there are two independent solutions of the Dirac equation for each set of quantum numbers. One of these solutions is irregular at the origin, and is therefore very difficult to determine accurately.

The same problem occurs in the solution of the Schrödinger equation at complex energies. To deal with this difficult problem we have found it convenient to use the phase method developed by Calogero (1963a). This has proved to be a numerically stable method of finding both the regular and irregular solutions of the Schrödinger equation. A good discussion of the phase method is given by Pinski (1984). Calogero (1963a, b) later generalised this method to be applicable to the usual radial Dirac equation. We have further generalised it for application to the problem of spin-polarised targets and hence to the four simultaneous radial equations of equation (3.6).

Let us begin by noting that the solutions of these radial Dirac equations satisfy:

$$\psi^{m_j}(\pm, E, r) = j_{l\pm}(\sqrt{Er}) - \int_0^r \mathrm{d}r' \,[V^{\mathrm{eff}}(r')\mathbf{I} - \boldsymbol{\sigma}_3 B^{\mathrm{eff}}(r')]$$
$$\times [j_{l\pm}(\sqrt{Er}) \otimes n_{l\pm}(\sqrt{Er}) - n_{l\pm}(\sqrt{Er}) \otimes j_{l\pm}(\sqrt{Er})] \cdot \mathbf{I} \cdot \boldsymbol{\psi}_l^{m_j}(\pm, E, r) \tag{5.2}$$

where $\times$ stands for inner product, $\otimes$ for outer product and $\cdot$ for matrix multiplication. The column vectors $J_{l\pm}$, $n_{l\pm}$ and $\psi_l^{m_j}$ are of the form:

$$\psi_l^{m_j}(\pm, E, r) = \begin{bmatrix} g_{\kappa_1\kappa}^{m_j^{\pm}} \\ \mathrm{if}_{\kappa_1\kappa}^{m^{\pm}} \\ g_{\kappa_2\kappa}^{m_j^{\pm}} \\ \mathrm{if}_{\kappa_2\kappa}^{m_j^{\pm}} \end{bmatrix} \qquad j_{l\pm}(x) = \begin{bmatrix} j_l(x) \\ \pm j_{l+1}(x) \\ j_l(x) \\ \pm j_{l-1}(x) \end{bmatrix} \qquad n_{l\pm}(x) = \begin{bmatrix} n_l(x) \\ \pm n_{l+1}(x) \\ n_l(x) \\ \pm n_{l-1}(x) \end{bmatrix} \tag{5.3}$$

where the $\pm$ refers to whether the solution is regular (+) or irregular (−) at the origin. Following Calogero we write the wavefunction as

$$\psi_l^m(\pm, E, r) = \begin{bmatrix} C_{\kappa_1\kappa}^{m_j}(\pm, E, r)\, j_l(\sqrt{Er}) - S_{\kappa_1\kappa}^{m_j}(\pm, E, r) n_l(\sqrt{Er}) \\ \dfrac{pc}{E+mc^2} S_{\kappa_1}[C_{\kappa_1\kappa}^{m_j}(\pm, E, r) j_{l+1}(\sqrt{Er})] - S_{\kappa_1\kappa}^{m_j}(\pm, E, r) n_{l+1}(\sqrt{Er}) \\ C_{\kappa_2\kappa}^{m_j}(\pm, E, r)\, j_l(\sqrt{Er}) - S_{\kappa_2\kappa}^{m_j}(\pm, E, r) n_l(\sqrt{Er}) \\ \dfrac{pc}{E+mc^2} S_{\kappa_2}[C_{\kappa_2\kappa}^{m_j}(\pm, E, r) j_{l-1}(\sqrt{Er})] - S_{\kappa_2\kappa}^{m_j}(\pm, E, r) n_{l-1}(\sqrt{Er}) \end{bmatrix}. \tag{5.4}$$

We can substitute this expression into (5.2) to find a set of four coupled differential equations for the coefficient functions $C_{\kappa_1\kappa}^{m_j}$, $C_{\kappa_2\kappa}^{m_j}$, $S_{\kappa_1\kappa}^{m_j}$ and $C_{\kappa_2\kappa}^{m_j}$. The resulting equations are unwieldy, but are straightforward to solve using the Adams–Bashforth method, for example. $C_{\kappa_1\kappa}^{m_j}$ and $S_{\kappa_1\kappa}^{m_j}$ are smooth functions in the muffin tin sphere, most of the infinity at the origin in the irregular part of the wavefunction has been swallowed up in the Neumann functions.

The regular solution of these equations is found by outward integration initialised by a series solution close to the origin. The irregular solution is found by inward integration starting at the muffin tin boundary. This is initialised by putting the wavefunction at the sphere radius Γ_{MT} equal to a spherical Bessel function as discussed by Pinski (1984). This procedure has been found to be numerically stable under all circumstances we have examined, and for the regular part we obtain the logarithmic derivative in at least five-figure agreement with other methods (Loucks 1967, for example).

5.3. The Brillouin zone integral for the site-diagonal τ-matrix

The τ-matrix is set up as shown in equation (4.8), with one atom per unit cell only and therefore

$$\tau_{\kappa m_j \kappa' m_j'}^{ii} = \frac{1}{\Omega} \int \mathrm{d}^3\boldsymbol{k}\, [t^{-1} - g(k, E)]^{-1}_{\kappa m_j \kappa' m_j'}. \tag{5.5}$$

For each value of the quantum numbers l and m_j, t is a 2×2 matrix. It is this 2×2 matrix that is inverted to find the elements of t^{-1} in contradistinction to the results of Schadler *et al*, whose method diverges in the non-relativistic limit! One can imagine the more general case of a field pointing in a general direction. Then m_j would no longer be a good quantum number and the t-matrix would then be the full $2(2l+1) \times 2(2l+1)$ matrix, and it is this that we would then have to invert.

With both spin–orbit coupling and spin-polarisation included in the calculation there are, in general, no remaining degeneracies and therefore it is necessary to solve the Dirac equation for every electron. This means solving the coupled Dirac equations 12 times. When $|m_j| = l + \frac{1}{2}$ we have only one element of the t-matrix that is diagonal in κ. If $|m_j| \neq l + \frac{1}{2}$ then there are two solutions diagonal in κ, one for each value of the J quantum number. Therefore the τ matrix is an 18×18 matrix for $l = 2$. However this matrix is rather sparse. Figures 1 and 2 show the structure and symmetry of τ in zero field in the κm_j and the *lms* representations, respectively. These figures are identical to those shown by Staunton *et al* (1980), as they should be, because they reflect the double point group symmetry of the cubic lattice (Onodera and Okazaki 1966). When a magnetic field is applied the symmetry is reduced and this is reflected in the symmetry of the τ-matrix in a finite field. This is shown for the $\kappa\mu$ representation (figure 3) and the *lms* representation (figure 4). There is a new s–d coupling introduced by the magnetic field, and splitting of many of the degeneracies.

κ \ κ'	m_j \ m_j'	-1		1		-2				2				-3					
		$-\frac{1}{2}$	$\frac{1}{2}$	$-\frac{1}{2}$	$\frac{1}{2}$	$-\frac{3}{2}$	$-\frac{1}{2}$	$\frac{1}{2}$	$\frac{3}{2}$	$-\frac{3}{2}$	$-\frac{1}{2}$	$\frac{1}{2}$	$\frac{3}{2}$	$-\frac{5}{2}$	$-\frac{3}{2}$	$-\frac{1}{2}$	$\frac{1}{2}$	$\frac{3}{2}$	$\frac{5}{2}$
-1	$-\frac{1}{2}$	A																	
	$\frac{1}{2}$		A																
1	$-\frac{1}{2}$			B															
	$\frac{1}{2}$				B														
-2	$-\frac{3}{2}$					C													
	$-\frac{1}{2}$						C												
	$\frac{1}{2}$							C											
	$\frac{3}{2}$								C										
2	$-\frac{3}{2}$									D					N				L
	$-\frac{1}{2}$										D					M			
	$\frac{1}{2}$											D					M		
	$\frac{3}{2}$												D	L				N	
-3	$-\frac{5}{2}$												L	G				P	
	$-\frac{3}{2}$									N					F				P
	$-\frac{1}{2}$										M					E			
	$\frac{1}{2}$											M					E		
	$\frac{3}{2}$												N	P				F	
	$\frac{5}{2}$									L					P				G

Figure 1. The matrix structure of $\tau(E)$ in the κm_j representation for a cubic crystal and zero magnetic moment.

S'			Up									Down									
		l'	0	1				2				0	1				2				
S	l	m \ m'	0	−1	0	1	−2	−1	0	1	2	0	−1	0	1	−2	−1	0	1	2
Up	0	0	A																	
	1	−1		D									K							
		0			B										K					
		1				C														
	2	−2					E				N							L			
		−1						G											M		
		0							H											M	
		1								J						P					L
		2					N				F						P				
Down	0	0										A									
	1	−1											C								
		0		K										B							
		1			K										D						
	2	−2								P						F					N
		−1					L				P						J				
		0						M										H			
		1							M										G		
		2								L						N					E

Figure 2. The matrix structure of $\tau(E)$ in the *lms* representation for a cubic crystal and zero magnetic moment.

Owing to the point group symmetry it is only necessary to perform the Brillouin zone integral in (5.5) in 1/48th of the Brillouin zone in the non-relativistic case. With the decrease in symmetry caused by the interplay between spin polarisation and spin–orbit coupling this is no longer sufficient. When a field is applied along a particular crystal axis, in our case the (0, 0, 1) z direction, we are making that direction inequivalent to the (1, 0, 0) and (0, 1, 0) directions. This decrease in symmetry means that it is necessary to perform the integration in 3/48ths of the zone with the field along (0, 0, 1). The segments of the BCC zone used in this case are shown in figure 5. The segments marked a, b and c were previously equivalent and are now inequivalent. Every time the moment points along a different direction it is necessary to recalculate the irreducible wedge of the zone. We have found that for an arbitrary direction of the field it is necessary to take $\frac{1}{4}$ of the zone in the integration of equation (5.5).

The actual method of doing this integration that was used throughout this paper is the prism method described in detail by Stocks *et al* (1979). The generalisation to more than 1/48th of the zone is straightforward. In the following section we display some densities of states curves for iron. As these were calculated for display purposes only high precision was not required and we have used six directions in each of the 1/48ths and approximately 250 k-points per direction.

κ' / κ \ $m_{j'}$ / m_j	−1	1	−2	2	−3
	$-\frac{1}{2}$ $\frac{1}{2}$	$-\frac{1}{2}$ $\frac{1}{2}$	$-\frac{3}{2}$ $-\frac{1}{2}$ $\frac{1}{2}$ $\frac{3}{2}$	$-\frac{3}{2}$ $-\frac{1}{2}$ $\frac{1}{2}$ $\frac{3}{2}$	$-\frac{5}{2}$ $-\frac{3}{2}$ $-\frac{1}{2}$ $\frac{1}{2}$ $\frac{3}{2}$ $\frac{5}{2}$
−1	$-\frac{1}{2}$ A			∇	α
	$\frac{1}{2}$ B			S	Z
1	$-\frac{1}{2}$	C	T		
	$\frac{1}{2}$	D	U		
−2	$-\frac{3}{2}$		E		
	$-\frac{1}{2}$	T	F		
	$\frac{1}{2}$	U	G		
	$\frac{3}{2}$		H		
2	$-\frac{3}{2}$			I	V θ
	$-\frac{1}{2}$ ∇			J	W
	$\frac{1}{2}$ S			K	X
	$\frac{3}{2}$			L	π Y
−3	$-\frac{5}{2}$			π	M Ξ
	$-\frac{3}{2}$			V	N Δ
	$-\frac{1}{2}$ α			W	O
	$\frac{1}{2}$ Z			X	P
	$\frac{3}{2}$			Y	Ξ Q
	$\frac{5}{2}$			θ	Δ R

Figure 3. The matrix structure of $\tau(E)$ in the κm_j representation for a cubic crystal where each site has a magnetic moment directed along (0, 0, 1).

Also shown in the following section are energy bands for iron. These were found from (5.5) by looking for the changes in the sign of the eigenvalues of the τ-matrix. It was found to be more efficient to look at eigenvalues than the determinant because then the degeneracy of the bands is automatically known.

6. Example: The electronic structure of ferromagnetic iron

In order to present as clear a picture as possible of the new effects introduced in a relativistic spin-polarised formalism, we have calculated the electronic structure of iron, with the magnetic moment pointing in different directions in the unit cell. The potential for this calculation was the result of a self-consistent, spin-polarised, non-relativistic electronic structure calculation (Moruzzi *et al* 1978). In that calculation there are spin up and spin down potentials, which are related to the input data for our calculation via

$$V^{\text{eff}}(r) = \tfrac{1}{2}[V\uparrow(r) + V\downarrow(r)] \tag{6.1a}$$

$$B^{\text{eff}}(r) = \tfrac{1}{2}[V\uparrow(r) - V\downarrow(r)]. \tag{6.1b}$$

Because iron is a fairly light ion we expect that the self-consistent potential in the non-relativistic regime will be close to that for relativistic case.

S	S'		Up									Down									
	l'		0	1			2					0	1			2					
	l	m \ m'	0	−1	0	1	−2	−1	0	1	2	0	−1	0	1	−2	−1	0	1	2
Up	0	0	A						T											U
	1	−1		B									θ							
		0			C										β					
		1				D														
	2	−2					E				W							∇		
		−1						F											ψ	
		0	T						G			X								Γ
		1								H							Y				Δ
		2					W				J							Z		
Down	0	0							X			K							α	
	1	−1											L							
		0		θ										M						
		1			β										N					
	2	−2								Y							O				π
		−1					∇				Z							P			
		0						ψ				α							Q		
		1	U						Γ											R	
		2								Δ							π				S

Figure 4. The matrix structure of $\tau(E)$ in the *lms* representation for a cubic crystal where each site has a magnetic moment directed along (0, 0, 1).

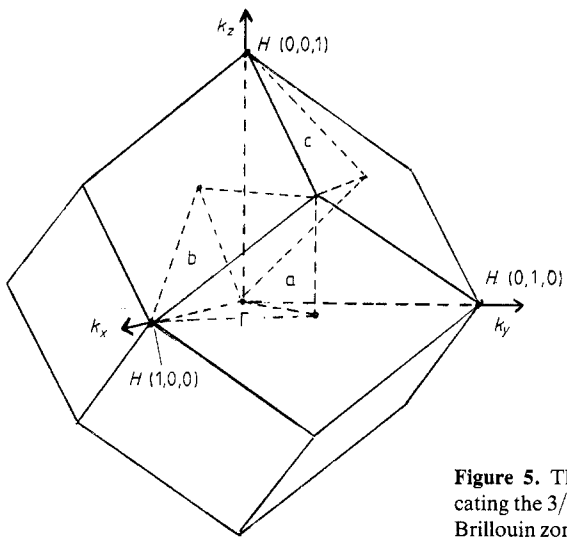

Figure 5. The BCC Brillouin zone, indicating the 3/48ths of the zone in which the Brillouin zone integral (5.5) is performed.

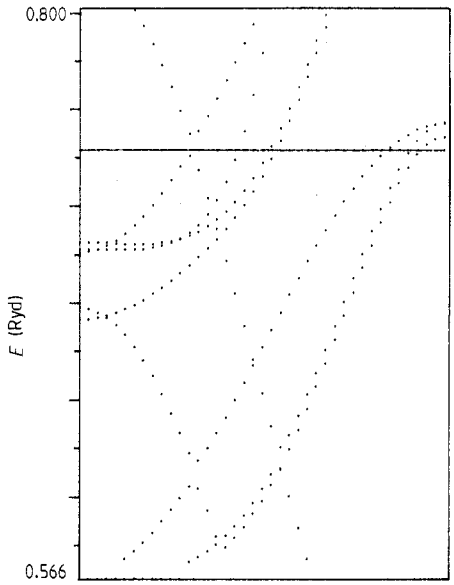

Figure 6. The energy band structure of iron along (0, 0, 1) with the magnetisation directed along (0, 0, 1).

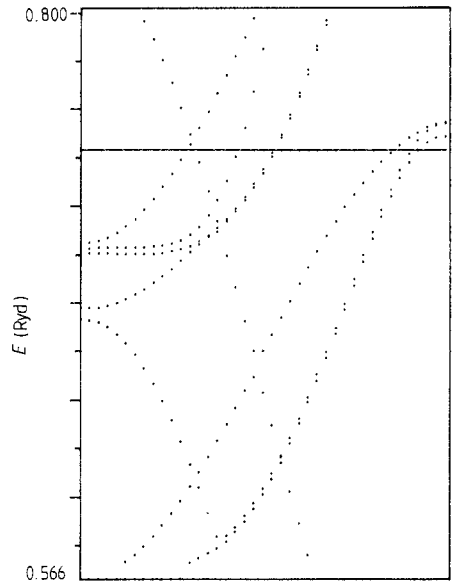

Figure 7. The energy band structure of iron along (1, 0, 0) with the magnetisation directed along (0, 0, 1).

First, we examine the energy bands of iron along (0, 0, 1) and (1, 0, 0) in the unit cell. In the non-relativistic case or in the relativistic case with no spin polarisation these directions would have identical bands, and as expected we essentially reproduce the energy bands of Moruzzi *et al*. However, figures 6 and 7 show the energy bands near E_F along Γ–H (001) and Γ–H (1, 0, 0), respectively, for the moment pointing along (0, 0, 1) in the unit cell. Figures 8 and 9 show bands along the same directions with the moment pointing along (1, 1, 0) and figures 10 and 11 are the same directions again with the magnetic moment along (1, 1, 1) in the unit cell. We see from these figures that inclusion of relativistic effects lifts degeneracies of bands at k-points of high symmetry and removes crossings of some bands which previously belonged to the two independent sets of 'spin-up' and 'spin-down' bands. This labelling of the bands is no longer possible as we are mixing spin character in the states, and this varies along the band. At points where crossings are avoided one cannot even say that the band is dominated by a particular spin direction. Another way of looking at this is to point out that the expectation value of σ_3 is no longer ± 1. The anisotropy in the bands leads to anisotropies in the Fermi surface. This is particularly noticeable in this example as there are bands which cross just above E_F in the non-relativistic case creating a very small piece of Fermi or hole surface. These are affected significantly by the anisotropy. It may be that for some directions of the moment the place where the bands cross, may cross the Fermi energy. Thus pieces of Fermi surface may be created or destroyed.

Figure 12 shows the density of states for iron with the magnetic moment pointing along the (0, 0, 1) direction. This, essentially, is a reproduction of the results of Moruzzi *et al* (1978). Comparison with their results shows that our density of states as some peaks taller and narrower than theirs. This is due to using only a few directions in the prism method for doing the Brillouin zone integration of equation (5.5). We could make our

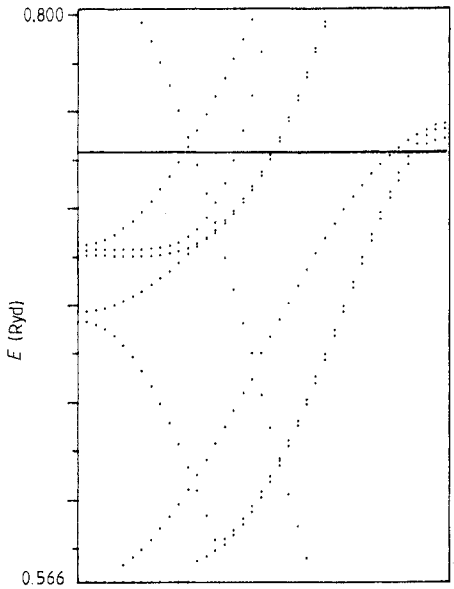

Figure 8. The energy band structure of iron along (0, 0, 1) with the magnetisation directed along (1, 1, 0).

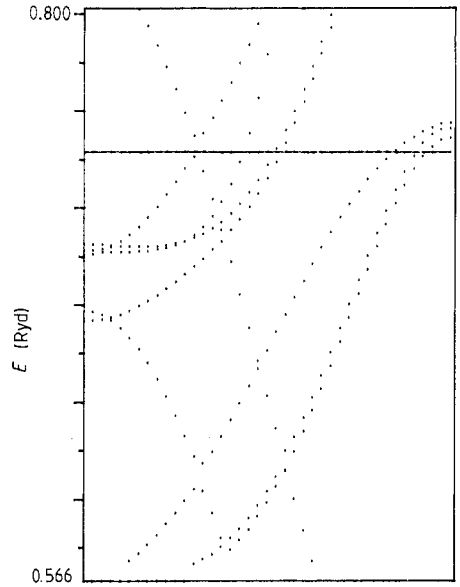

Figure 9. The energy band structure of iron along (1, 0, 0) with the magnetisation directed along (1, 1, 0).

results more like theirs by using a larger number of directions. However, for the present illustrative purposes the extra effort does not seem to be justified.

Figure 13 shows the density of states of iron just below the Fermi energy. The full line shows the density of states for the moment along (0, 0, 1) and the broken line is for

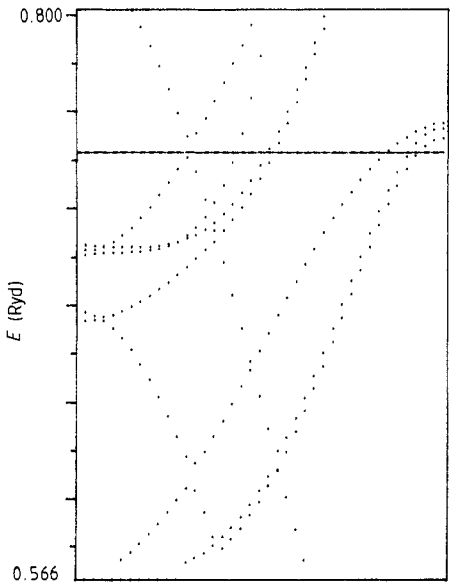

Figure 10. The energy band structure of iron along (0, 0, 1) with the magnetisation directed along (1, 1, 1).

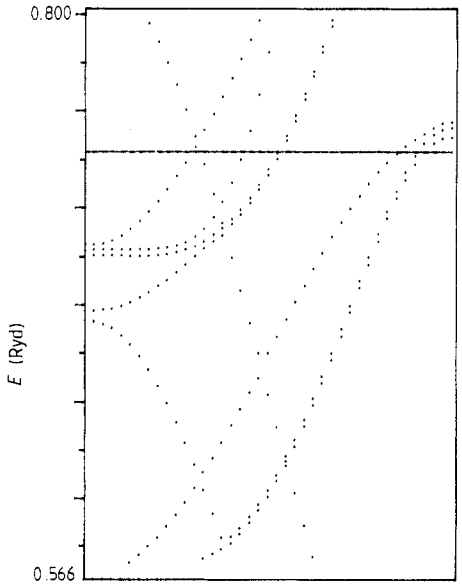

Figure 11. The energy band structure of iron along (1, 0, 0) with the magnetisation directed along (1, 1, 1).

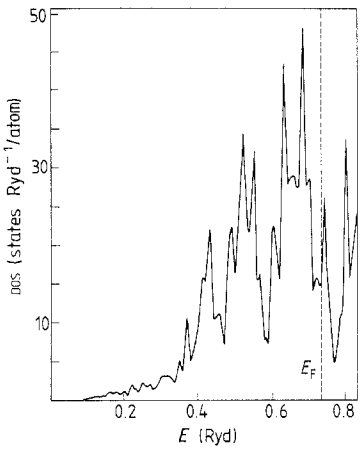

Figure 12. The density of states of iron.

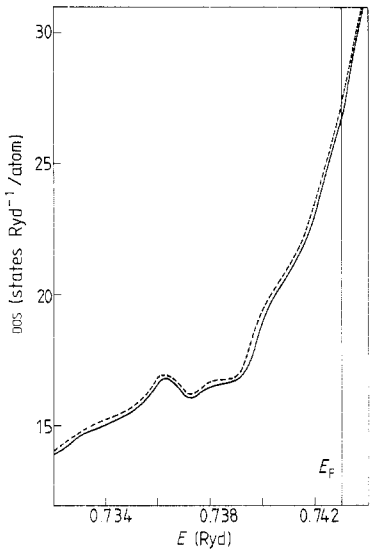

Figure 13. The density of states of iron just below E_F for the magnetic direction pointing along (0, 0, 1) (full line), and (1, 1, 0) (dashed line). The density of states for the moment along (1, 1, 1) falls on top of the full line on this scale. The Fermi energy is the one calculated for the moment along (0, 0, 1) and is only calculated to a precision of ±1 mRyd.

the moment along (1, 1, 0). The density of states for the moment along (1, 1, 1) falls directly on top of the (0, 0, 1) curve on this scale. The Fermi energy on this diagram is for the moment along (0, 0, 1) and will clearly change for different moment directions.

Finally we have calculated the spin contribution to the magnetic moment of iron using (4.10). Decomposed by l quantum number, these are ($l = 0$; $\mu = -0.010\ \mu_B$), ($l = 1$; $\mu = -0.047\ \mu_B$) and ($l = 2$; $\mu = 2.140$), which is in very satisfactory agreement with the calculation of Moruzzi *et al* (1978).

7. Conclusions

A relativistic spin-polarised multiple-scattering theory has been developed which treats spin polarisation and spin–orbit coupling on an equal footing. Computationally convenient expressions for the scattering Green functions have been found. The method has been applied to a calculation of the electronic structure of iron.

From figure 13 we can see that there are differences in densities of states for the moment pointing along different directions in the unit cell. This leads us to hope that magnetocrystalline anisotropy energies may be given approximately by the difference in the single-electron energies. This constitutes a method of calculating the easy axis of magnetisation from first principles.

We have also noted that the single-electron energies show most difference, for different directions of the moment, at peaks in $N(E)$. Looking at the energy bands we see that this tends to be at the centre or boundary of the Brillouin zone. Therefore, it is tempting to suggest that for a given band, its contribution to the anisotropy energy will

be largest when $\partial^2 E/\partial k^2$ is a maximum, i.e., the magnetocrystalline anisotropy energy is inversely proportional to the band mass.

That the difference in single-electron energies is calculable within this theory means we can also hope to interpret other experiments such as the difference in the x-ray absorption spectrum of ferromagnetic metals of left or right circularly polarised incident photons. Work is in progress on these topics.

Acknowledgments

One of us (PS) would like to thank SERC for a postdoctoral fellowship during which the work described in this paper was done.

References

Calogero F 1963a *Nuovo Cimento* **27** 261
—— 1963b *Nuovo Cimento* **27** 1007
Davis H L 1971 *Computational Methods in Band Theory* ed. P M Marcus, J F Janak and A R Williams (New York: Plenum)
Ebert H and Gyorffy B L 1987 *J. Phys. F: Met. Phys.* **18** 451
Faulkner J S and Stocks G M 1980 *Phys. Rev.* B **21** 3222
Feder R 1985 *Polarised Electrons in Surface Physics* ed. R Feder (Singapore: World Scientific Publishing)
Feder R, Rosicky F and Ackermann B 1983 *Z. Phys.* B **52** 31
Gyorffy B L and Stott M J 1973 *Band Structure Spectroscopy of Metals and Alloys* ed. D J Fabian and L M Watson (New York: Academic)
Hedin L and Lundqvist B I 1971 *J. Phys. C: Solid State Phys.* **4** 2064
Koenig C 1973 *J. Phys. F: Met. Phys.* **3** 1497
Kohn W and Vashista P 1983 *Theory of the Inhomogeneous Electron Gas* ed. S Lundqvist and N H March (New York: Plenum)
Korringa J 1947 *Physica* **13** 392
Landau L D, Lifshitz E M and Pitaevskii L P 1984 *Electrodynamics of Continuous Media* 2nd edn, *Landau and Lifshitz Course in Theoretical Physics* (New York: Pergamon)
Lloyd P and Smith P V 1972 *Adv. Phys.* **21** 89
Loucks T L 1967 *The Augmented Plane Wave Method* (New York: Benjamin)
MacDonald A H and Vosko S H 1979 *J. Phys. C: Solid State Phys.* **12** 2977
March N H, Lambin P H and Herman F 1984 *J. Magn. Magn. Mater.* **44** 1
Morruzi V L, Janak J F and Williams A R 1978 *Calculated Electronic Properties of Metals* (Oxford: Pergamon)
Onodera Y and Okazaki M 1966 *J. Phys. Soc. Japan* **21** 1273
Pendry J B 1974 *Low Energy Electron Diffraction* (New York: Academic)
Pinski F J 1984 *J/ψ Newsletter No 8* ed. P Strange and W M Temmerman (Daresbury Laboratory), p 27
Rajagopal A K 1978 *J. Phys. C: Solid State Phys.* **11** L943
Ramana M V and Rajagopal A K 1979 *J. Phys. C: Solid State Phys.* **12** L845
Rose M E 1961 *Relativistic Electron Theory* (New York: Wiley)
Schadler G, Boring A M, Albers R C and Weinberger P 1987 *Phys. Rev.* B **35** 4324
Schutz G, Wagner W, Wilhelm W, Kienle P, Zeller R, Frahm R and Materlik G 1987 *Phys. Rev. Lett.* **58** 737
Staunton J B, Gyorffy B L and Weinberger P 1980 *J. Phys. F: Met. Phys.* **10** 2665
Staunton J B, Poulter J, Gyorffy B L and Strange P 1988 *J. Phys. C: Solid State Phys.* **21** 1595
Stocks G M, Temmerman W M and Winter H 1979 *Electrons in Disordered Metals and at Metallic Surfaces* (Nato ASI Series B, vol 42) (New York: Plenum)
Stocks G M and Winter H 1984 in *The Electronic Structure of Complex Systems* (Nato ASI Series B, vol 113) (New York: Plenum)
Strange P, Poulter J, Virji H, Staunton J B and Gyorffy B L 1987 *J/ψ Newsletter No 11,* ed. P Strange and W M Temmerman (Daresbury Laboratory), p 2
Strange P, Staunton J B and Gyorffy B L 1984 *J. Phys. C: Solid State Phys.* **17** 3355
Zeller R, Deutz J and Dederichs P H 1982 *Solid State Commun.* **44** 993